

# Double-spin asymmetries for small- $Q_T$ Drell-Yan pair production in transversely polarized $p\bar{p}$ collisions

HIROYUKI KAWAMURA<sup>a</sup>, JIRO KODAIRA<sup>b\*</sup> AND KAZUHIRO TANAKA<sup>c</sup>

<sup>a</sup> *Radiation Laboratory, RIKEN, Wako 351-0198, Japan*

<sup>b</sup> *Theory Division, KEK, Tsukuba 305-0801, Japan*

<sup>c</sup> *Department of Physics, Juntendo University, Inba, Chiba 270-1695, Japan*

## Abstract

We discuss the Drell-Yan process at a measured transverse-momentum  $Q_T$  of the produced lepton pair in collisions of transversely polarized protons and antiprotons, to be observed at the proposed spin experiments at GSI. The large logarithmic contributions from multiple soft gluon emission, accompanying the Drell-Yan mechanism at small  $Q_T$ , are resummed to all orders in QCD perturbation theory up to next-to-leading logarithmic (NLL) accuracy. Numerical evaluation shows the impact of the NLL as well as LL effect on the dilepton  $Q_T$  spectra. For the corresponding  $Q_T$ -dependent spin asymmetry  $\mathcal{A}_{TT}(Q_T)$ , the LL effect gives significant modification while the NLL effect is marginal, leading to QCD prediction that  $\mathcal{A}_{TT}(Q_T)$  at GSI is flat at small and moderate  $Q_T$  and almost equals the conventional asymmetry  $A_{TT}$  associated with the  $Q_T$ -integrated cross sections. This flat behavior in turn allows us to use analytic saddle-point evaluation of the resummation formula in the limit  $Q_T \rightarrow 0$ , not only to obtain quantitative estimate of  $\mathcal{A}_{TT}(Q_T)$ , but also to clarify mechanisms behind the relation  $\mathcal{A}_{TT}(Q_T) \simeq A_{TT}$  characteristic of  $p\bar{p}$  collisions at GSI.

---

\*Deceased.

Recently there has been much progress to unveil the last unknown parton distribution of nucleon at the leading twist, the transversity distribution  $\delta q(x)$  [1, 2]: for example, the calculation of the lowest two moments of  $\delta q(x)$  by lattice QCD simulation is updated [3], and the first global fit of  $\delta q(x)$  is given [4] using the semi-inclusive deep inelastic scattering (SIDIS) data, in combination with the  $e^+e^-$  data for the associated (Collins) fragmentation function. These results indicate that the transversity distributions for  $u$  and  $d$  quarks are sizable, but are fairly small compared with their positivity bound (Soffer bound) [5]; still, these results are subject to certain assumptions and uncertainties, and it is important to proceed further toward the determination of the transversity.

As is well-known [1, 2], the transversely polarized Drell-Yan (tDY) process provides another promising way to access  $\delta q(x)$ . The measurement of the tDY cross section is proposed in the future experiments at GSI [6], where the  $p\bar{p}$  collisions at moderate energy mainly probes the products of two quark transversity-distributions,  $\delta q(x_1)\delta q(x_2)$ , in the “valence region”. The corresponding double-spin asymmetries estimated at the leading order (LO) in QCD are large enough to be measured at GSI [7], in contrast to the complementary case of tDY in  $pp$  collisions at RHIC, where the asymmetries are predicted to be rather small because  $\delta q(x_1)\delta\bar{q}(x_2) + (1 \leftrightarrow 2)$  is probed in the “sea-quark region” (see [8, 9, 10]). As for the higher-order QCD corrections for tDY in  $p\bar{p}$  collisions, the NLO corrections have been studied recently [11]; also, the “threshold resummation” has been applied in order to sum up, to all orders in  $\alpha_s$ , the soft-gluon emission contributions that are logarithmically enhanced near the threshold of the partonic process [12]. The effects of these QCD corrections are small for the double transverse-spin asymmetries in  $p\bar{p}$  collisions at the kinematical regions corresponding to the GSI experiments [11, 12], suggesting that the large LO asymmetries obtained in [7] are rather robust.

All the above previous studies of tDY in  $p\bar{p}$  collisions considered the case in which the transverse-momentum  $Q_T$  of the produced lepton pair are unobserved. Experimentally, however, the bulk of events is produced in the small  $Q_T$  region. Therefore, it is desirable to develop theoretical predictions of tDY at a measured  $Q_T$  in  $p\bar{p}$  collisions for the detailed comparison with the data in the future GSI experiments. When  $Q_T \ll Q$  with  $Q$  the dilepton mass, the fixed-order perturbation theory breaks down due to the appearance of large logarithms  $\ln(Q^2/Q_T^2)$  multiplying  $\alpha_s$ , and we have to deal with the relevant DY cross sections at small  $Q_T$  in an all-order resummation framework in QCD. The corresponding “ $Q_T$ -resummation” has formally some resemblance to the threshold resummation mentioned above, but represents other contributions associated with different “edge region” of phase space. The  $Q_T$ -resummation for tDY has been formulated recently by the present authors [13, 9, 10], summing the corresponding large logarithms up to next-to-leading logarithmic (NLL) accuracy, in the context of the  $pp$  collisions at RHIC and J-PARC. There we demonstrated that profound modifications arise in the DY production at small  $Q_T$ , driven by partonic mechanism that induces the large logarithmic contributions; in particular, the interplay between the Sudakov factor resumming multiple soft gluon emission and the DGLAP evolutions of parton distributions yields the “amplification” of the double transverse-spin asymmetries in the small  $Q_T$  region at RHIC as well as J-PARC kinematics, resulting in their values larger than the conventional (fixed-order) NLO asymmetries

[8] calculated in the  $Q_T$ -unobserved case. In this Letter we apply our  $Q_T$ -resummation formalism to the case of  $p\bar{p}$  collisions, and study the corresponding double transverse-spin asymmetries in the small  $Q_T$  region for tDY foreseen at GSI.

Detailed derivation of the tDY cross sections in our  $Q_T$  resummation formalism is given in [10] for collisions of spin-1/2 hadrons  $h_1$  and  $h_2$ , i.e.,  $h_1 h_2 \rightarrow l^+ l^- X$ , and the corresponding results for  $p\bar{p}$  collisions can be obtained by trivial substitutions. The spin-dependent ( $\Delta_T d\sigma \equiv (d\sigma^{\uparrow\uparrow} - d\sigma^{\uparrow\downarrow})/2$ ) and spin-independent ( $d\sigma \equiv (d\sigma^{\uparrow\uparrow} + d\sigma^{\uparrow\downarrow})/2$ ) parts of the differential cross section are expressed as

$$\frac{(\Delta_T) d\sigma}{dQ^2 dQ_T^2 dy d\phi} = (\cos(2\phi)/2) \frac{2\alpha^2}{3 N_c S Q^2} \left[ (\Delta_T) \tilde{X}^{\text{NLL}}(Q_T^2, Q^2, y) + (\Delta_T) \tilde{Y}(Q_T^2, Q^2, y) \right]. \quad (1)$$

Here and below we follow the convention of [9, 10] for the basic quantities entering the formulae:  $\sqrt{S}$  and  $y$  are the total energy and dilepton's rapidity in the proton-antiproton CM system, and the prefactor  $\cos(2\phi)/2$  specific to the spin-dependent part shows the characteristic dependence [1] on the azimuthal angle  $\phi$  of one of the outgoing leptons with respect to the incoming nucleon's spin axis. The first term ( $\Delta_T \tilde{X}^{\text{NLL}}$  or  $\tilde{X}^{\text{NLL}}$ ) gives the dominant contribution when  $Q_T \ll Q$ , containing all the logarithmically-enhanced contributions  $\alpha_s^n \ln^m(Q^2/Q_T^2)/Q_T^2$  and, at the NLL accuracy, has to be evaluated by resumming the first three towers ( $m = 2n - 1, 2n - 2, 2n - 3$ ) of these large logarithmic contributions to all orders in  $\alpha_s$ . The second term ( $\Delta_T \tilde{Y}$  or  $\tilde{Y}$ ) is free of such contributions, and can be computed by fixed-order truncation of the perturbation theory.

The NLL resummed component  $(\Delta_T) \tilde{X}^{\text{NLL}}$  is obtained through various kinds of elaboration [13, 9, 10, 14, 15] of the Collins-Soper-Sterman (CSS) resummation formalism [16]. Introducing the impact parameter  $b$  space, which is conjugate to the  $Q_T$  space, we have\*

$$\begin{aligned} \Delta_T \tilde{X}^{\text{NLL}}(Q_T^2, Q^2, y) = & \int_C db \frac{b}{2} J_0(bQ_T) e^{S(b,Q) - g_{NP} b^2} \left[ \delta H \left( x_1^0, x_2^0; \frac{b_0^2}{b^2} \right) \right. \\ & \left. + \frac{\alpha_s(Q^2)}{2\pi} \left\{ \int_{x_1^0}^1 \frac{dz}{z} \Delta_T C_{qq}^{(1)}(z) \delta H \left( \frac{x_1^0}{z}, x_2^0; \frac{b_0^2}{b^2} \right) + (x_1^0 \leftrightarrow x_2^0) \right\} \right], \end{aligned} \quad (2)$$

$$\begin{aligned} \tilde{X}^{\text{NLL}}(Q_T^2, Q^2, y) = & \int_C db \frac{b}{2} J_0(bQ_T) e^{S(b,Q) - g_{NP} b^2} \left[ H \left( x_1^0, x_2^0; \frac{b_0^2}{b^2} \right) \right. \\ & \left. + \frac{\alpha_s(Q^2)}{2\pi} \left\{ \int_{x_1^0}^1 \frac{dz}{z} C_{qq}^{(1)}(z) H \left( \frac{x_1^0}{z}, x_2^0; \frac{b_0^2}{b^2} \right) + \int_{x_1^0}^1 \frac{dz}{z} C_{qq}^{(1)}(z) K \left( \frac{x_1^0}{z}, x_2^0; \frac{b_0^2}{b^2} \right) + (x_1^0 \leftrightarrow x_2^0) \right\} \right], \end{aligned} \quad (3)$$

where the DY scaling variables are denoted as  $x_1^0 = \sqrt{Q^2/S} e^y$  and  $x_2^0 = \sqrt{Q^2/S} e^{-y}$ ,  $J_0(bQ_T)$  is a Bessel function, and  $b_0 = 2e^{-\gamma_E}$  with  $\gamma_E$  the Euler constant.  $\delta H$ ,  $H$ , and  $K$  denote the products of the NLO parton distributions of proton and antiproton, summed over the massless quark flavors  $q$  with their charge squared  $e_q^2$ , as

$$(\delta)H(x_1, x_2; \mu^2) = \sum_q e_q^2 [(\delta)q(x_1, \mu^2)(\delta)q(x_2, \mu^2) + (\delta)\bar{q}(x_1, \mu^2)(\delta)\bar{q}(x_2, \mu^2)] \quad (4)$$

---

\* In this paper, we set  $\mu_R = \mu_F = Q$  for the renormalization and factorization scales  $\mu_R$  and  $\mu_F$ .

and  $K(x_1, x_2; \mu^2) = \sum_q e_q^2 g(x_1, \mu^2) [q(x_2, \mu^2) + \bar{q}(x_2, \mu^2)]$ , where  $\delta q(x, \mu^2)$ ,  $q(x, \mu^2)$ , and  $g(x, \mu^2)$  are the quark transversity, quark density, and gluon density distributions of the proton, respectively; note that there is no transversely-polarized gluon distribution at the leading twist. The Sudakov factor  $e^{S(b, Q)}$  and the coefficient functions  $(\Delta_T)C_{ij}^{(1)}(z)$  are perturbatively calculable, and the former gives the all-order resummation of logarithmically enhanced contributions due to multiple emission of soft and/or collinear gluons from the incoming partons. The exponent  $S(b, Q)$  is expressed as

$$S(b, Q) = \frac{1}{\alpha_s(Q^2)} h^{(0)}(\lambda) + h^{(1)}(\lambda), \quad (5)$$

where the first and second terms collect the LL and NLL contributions, respectively, in terms of the two functions  $h^{(0)}(\lambda)$  and  $h^{(1)}(\lambda)$ , which depend on  $\alpha_s(Q^2)$  only through

$$\lambda = \beta_0 \alpha_s(Q^2) \ln(Q^2 b^2 / b_0^2 + 1) \equiv \beta_0 \alpha_s(Q^2) \tilde{L}, \quad (6)$$

with  $\beta_0$  the first coefficient of the QCD  $\beta$  function. When  $Q_T \ll Q$ ,  $\tilde{L}$  plays the role of the large-logarithmic expansion parameter in the  $b$  space, as  $b \sim 1/Q_T$ . In this relevant region,  $\lambda$  can be as large as 1 even for  $\alpha_s(Q^2) \ll 1$ , and the ratio of two terms in (5) is of  $\mathcal{O}(\alpha_s)$ ; note that the NNLL or higher-level corrections, which are down by  $\alpha_s$  or more, are neglected in (5) [9, 10]. The Sudakov exponent is independent of process as well as scheme to the NLL accuracy [13, 14, 17], so that (5) gives the universal Sudakov factor common to (2) and (3). The explicit form of  $h^{(0)}(\lambda)$  and  $h^{(1)}(\lambda)$ , as well as the coefficient functions  $(\Delta_T)C_{ij}^{(1)}(z)$  in the  $\overline{\text{MS}}$  scheme, can be found in [13, 9, 10]. It is implicit in (2) and (3) that the  $b$  dependence of  $\delta H(x_1, x_2; b_0^2/b^2)$ ,  $H(x_1, x_2; b_0^2/b^2)$  and  $K(x_1, x_2; b_0^2/b^2)$ , associated with the NLO perturbative evolution of the parton distributions from the factorization scale  $\mu_F = Q$  to the scale  $b_0/b$ , is also organized in terms of (6) to ensure the consistent NLL accuracy; i.e., the customary NLO evolution operators for the distributions are expanded up to the NLL term, where the LL term proves to be absent [9, 10]. The Fourier transformation to the  $Q_T$  space in (2), (3) is performed along a contour  $\mathcal{C}$  in the complex  $b$  space [9, 10, 15, 14], avoiding the singularity of the Sudakov exponent (5) at  $\lambda = 1$ , which is associated with the Landau pole in the perturbative running coupling. This singularity in the  $b$  space signals the onset of additional nonperturbative phenomena at very large values of  $|b|$ , and the corresponding nonperturbative effects are complemented in (2), (3) by introducing a Gaussian smearing function  $\exp(-g_{NP} b^2)$  with a parameter  $g_{NP}$ , following the usual procedure [13, 14, 15, 16]. This may be interpreted as representing ‘‘intrinsic transverse momentum’’ of partons inside proton, and we use the same smearing function for both polarized and unpolarized cases, following our previous works [9, 10] for tDY in  $pp$  collisions.

The ‘‘regular component’’  $(\Delta_T)\tilde{Y}$  is determined by the matching procedure expanding (2), (3) in powers of  $\alpha_s(Q^2)$  and assuming  $g_{NP} \rightarrow 0$  in perturbation theory, so that (1) coincides exactly with the fixed-order result of the corresponding polarized and unpolarized differential cross sections, up to  $\mathcal{O}(\alpha_s)$  [13, 15, 14]. Namely, the LO cross section for  $Q_T > 0$ ,  $(\Delta_T)d\sigma^{\text{LO}}/dQ^2 dQ_T^2 dy d\phi$ , which is of  $\mathcal{O}(\alpha_s)$  because the finite  $Q_T$  of the lepton pair is provided by the recoil from the gluon radiation, is given by (1) with the replacement  $(\Delta_T)\tilde{X}^{\text{NLL}} \rightarrow (\Delta_T)\tilde{X}^{\text{NLL}}|_{\text{FO}}$ , where  $(\Delta_T)\tilde{X}^{\text{NLL}}|_{\text{FO}}$  denotes the terms resulting from

the expansion of the resummed expression up to the fixed-order  $\alpha_s(Q^2)$ . According to the structure of (1) via the matching with the LO cross sections, we refer to (1) as the “NLL+LO” prediction, and this gives the tDY differential cross sections in the  $\overline{\text{MS}}$  scheme, which are well-defined over the entire range of  $Q_T$ .

The ratio from (1) yields the double transverse-spin asymmetry in tDY as

$$\mathcal{A}_{TT}(Q_T) = \frac{1}{2} \cos(2\phi) \frac{\Delta_T \tilde{X}^{\text{NLL}}(Q_T^2, Q^2, y) + \Delta_T \tilde{Y}(Q_T^2, Q^2, y)}{\tilde{X}^{\text{NLL}}(Q_T^2, Q^2, y) + \tilde{Y}(Q_T^2, Q^2, y)}, \quad (7)$$

for measured  $Q_T$ ,  $Q$ ,  $y$ , and  $\phi$ . To the fixed-order  $\alpha_s$  without the soft gluon resummation,  $(\Delta_T) \tilde{X}^{\text{NLL}} \rightarrow (\Delta_T) \tilde{X}^{\text{NLL}}|_{\text{FO}}$  as discussed above, and (7) reduces to the LO prediction  $\mathcal{A}_{TT}^{\text{LO}}(Q_T)$  for  $Q_T > 0$ . We also introduce the asymmetry in terms of the NLL resummed components, (2) and (3), which, respectively, dominate the numerator and denominator in (7) when  $Q_T \ll Q$ :

$$\mathcal{A}_{TT}^{\text{NLL}}(Q_T) = \frac{1}{2} \cos(2\phi) \frac{\Delta_T \tilde{X}^{\text{NLL}}(Q_T^2, Q^2, y)}{\tilde{X}^{\text{NLL}}(Q_T^2, Q^2, y)}. \quad (8)$$

As emphasized in [9, 10] in the context of the  $pp$  collisions, the  $Q_T \rightarrow 0$  limit of (2) and (3) deserves special attention: at  $Q_T = 0$ , the  $b$  integral of (2) and (3) is controlled by a saddle point and can be evaluated analytically as

$$(\Delta_T) \tilde{X}^{\text{NLL}}(0, Q^2, y) = \left[ \frac{b_0^2}{4Q^2 \beta_0 \alpha_s(Q^2)} \sqrt{\frac{2\pi}{\zeta^{(0)''}(\lambda_{SP})}} e^{-\zeta^{(0)}(\lambda_{SP}) + h^{(1)}(\lambda_{SP})} \right] (\delta) H \left( x_1^0, x_2^0; \frac{b_0^2}{b_{SP}^2} \right), \quad (9)$$

where  $\zeta^{(0)}(\lambda) \equiv -\lambda/[\beta_0 \alpha_s(Q^2)] - h^{(0)}(\lambda)/\alpha_s(Q^2) + [g_{NP} b_0^2/Q^2] e^{\lambda/[\beta_0 \alpha_s(Q^2)]}$ , and the saddle-point value of (6)<sup>†</sup>,  $\lambda_{SP} = \beta_0 \alpha_s(Q^2) \ln(Q^2 b_{SP}^2/b_0^2)$ , is defined by the condition  $\zeta^{(0)'}(\lambda_{SP}) = 0$ . The saddle-point formula (9) is exact up to the  $\mathcal{O}(\alpha_s)$  corrections that actually correspond to the NNLL contributions in the region  $Q_T \approx 0$  (see the discussion below (6), and also [9, 10] for the details). Note that the gluon distribution completely decouples from  $\tilde{X}^{\text{NLL}}(0, Q^2, y)$  at the NLL accuracy for  $Q_T \approx 0$ . The prefactor inside the square bracket in the RHS involves “large perturbative effects” due to the Sudakov factor, as well as the Gaussian smearing factor with  $g_{NP}$ ; the former contribution drives the well-known asymptotic behavior [18] of the DY cross sections,  $\sim (\Lambda_{\text{QCD}}^2/Q^2)^{a \ln(1+1/a)}$  with  $a \equiv A_q^{(1)}/(2\pi\beta_0)$ , for  $Q \gg \Lambda_{\text{QCD}}$ . Because this prefactor is common to both the polarized and unpolarized cross sections, we obtain the remarkably compact formula for the  $Q_T \rightarrow 0$  limit of (8) [9, 10]:

$$\mathcal{A}_{TT}^{\text{NLL}}(Q_T = 0) = \frac{1}{2} \cos(2\phi) \frac{\delta H(x_1^0, x_2^0; b_0^2/b_{SP}^2)}{H(x_1^0, x_2^0; b_0^2/b_{SP}^2)}. \quad (10)$$

Using the formulae described above, we study the behavior of tDY to be observed in  $p\bar{p}$  collisions at GSI. The PAX Collaboration has proposed the tDY experiments in  $p\bar{p}$  collisions

---

<sup>†</sup> For the kinematics of our interest, we have the saddle point well above  $b = 0$ , and we can use the definition  $\lambda = \beta_0 \alpha_s(Q^2) \ln(Q^2 b^2/b_0^2)$ , up to the exponentially suppressed corrections to (9) (see [9, 10]).

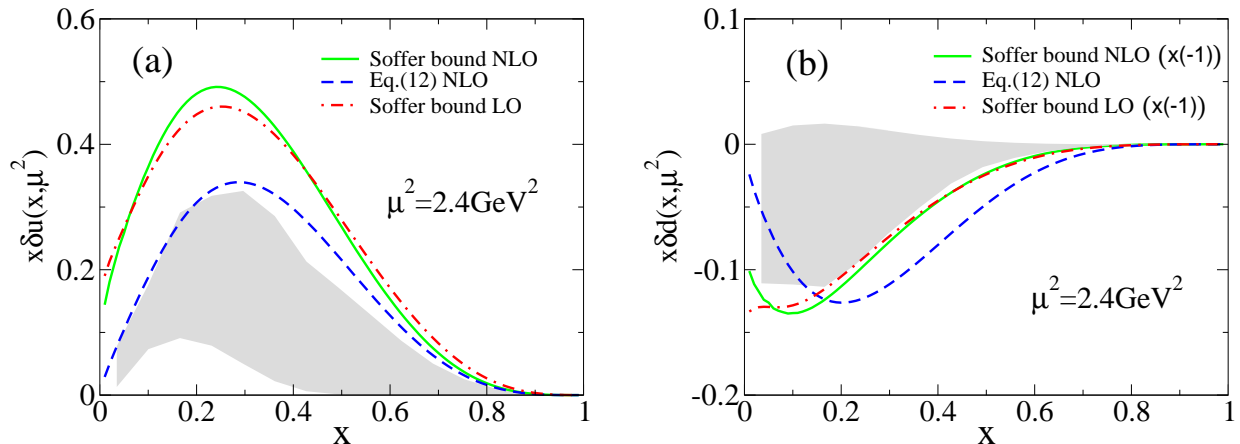


Figure 1: The transversity distributions for (a)  $u$ -quark and (b)  $d$ -quark. The solid and dashed curves plot the NLO distributions corresponding to the Soffer bound and the relation (11), respectively. The dot-dashed curve shows the LO distribution corresponding to the Soffer bound and the shaded area shows the result of the LO global fit in [4].

at  $S = 30$  and  $45 \text{ GeV}^2$  in the fixed-target mode, and those up to  $S = 210 \text{ GeV}^2$  in the collider mode [6]. Those GSI-PAX experiments will probe  $0.2 \lesssim Q/\sqrt{S} \lesssim 0.7$ , and thus the transversities in the “valence region” in a wide range of  $x$ . To compute the tDY cross sections (1) at the NLL+LO accuracy with these GSI kinematics, we have to specify the NLO parton distributions to be substituted. We use the NLO GRV98 distributions [19] for the unpolarized quark and gluon distributions  $q(x, \mu^2)$  and  $g(x, \mu^2)$ . For the NLO transversity distributions  $\delta q(x, \mu^2)$ , we consider the two typical assumptions that have been used in the literature [2, 7, 8, 13, 9, 10, 11, 12]: at a low input scale  $\mu_0 \lesssim 1 \text{ GeV}$ , these assume the saturation of Soffer’s inequality [5] as  $\delta q(x, \mu_0^2) = [q(x, \mu_0^2) + \Delta q(x, \mu_0^2)]/2$ , and the relation,

$$\delta q(x, \mu_0^2) = \Delta q(x, \mu_0^2) , \quad (11)$$

exact in the non-relativistic limit, respectively, and their QCD evolution from  $\mu_0$  to a higher scale  $\mu$  is controlled by the NLO DGLAP kernel [21] for the transversity; here  $\Delta q(x, \mu_0^2)$  denote the longitudinally polarized quark distributions. The first case yields  $\delta q(x, \mu^2)$  that satisfies Soffer’s inequality<sup>‡</sup> and provides an upper bound on the transversities [8]. The second case (11) is suggested also by the estimates from relativistic quark models for nucleon [2, 7, 22]. For the input functions in the RHS of these two assumptions, we take the NLO GRV98 distributions  $q(x, \mu_0^2)$ , as noted above, and GRSV2000 (“standard scenario”) distributions  $\Delta q(x, \mu_0^2)$  [20] with  $\mu_0^2 = 0.40 \text{ GeV}^2$ . The obtained NLO transversity distributions for  $u$  and  $d$  quarks,  $x\delta u(x, \mu^2)$  and  $x\delta d(x, \mu^2)$ , are shown in Figs. 1 (a) and (b), respectively, as a function of  $x$  with  $\mu^2 = 2.4 \text{ GeV}^2$ . The solid curve shows the result corresponding to the Soffer bound, and the dashed curve shows the result using (11). For comparison, we also depict the shaded area which represents the result (a one-sigma

<sup>‡</sup> The obtained  $\delta q(x, \mu^2)$  is actually very close to  $[q(x, \mu^2) + \Delta q(x, \mu^2)]/2$ , except for small  $x$  ( $\lesssim 0.2$ ).

confidence interval) for the LO transversity distributions extracted through the global fit to the data [4], and the dot-dashed curve which shows the LO transversity distributions corresponding to the Soffer bound with the LO inputs of [19, 20]. We note that the above assumption for the Soffer bound,  $\delta q(x, \mu_0^2) = [q(x, \mu_0^2) + \Delta q(x, \mu_0^2)]/2$ , following the literature [8, 13, 9, 10, 11, 12] yields the positive polarization for the  $d$  quark,  $\delta d(x, \mu^2) > 0$ , in contrast to the result using (11), but the sign of the polarization cannot be detected in tDY for  $p\bar{p}$  collision (see (4)). For convenience of comparison, the solid and dot-dashed curves in Fig. 1(b) show the results multiplied by  $-1$ .

The results in Figs. 1 (a) and (b) indicate that the empirical LO transversities are smaller compared with the transversities corresponding to the Soffer bound, in particular for the  $u$  quark. On the other hand, the NLO transversities using (11) lie slightly outside the one-sigma error bounds of the empirical fit. The two NLO sets as well as the empirical fit have  $(\delta u(x, \mu^2))^2 \gg (\delta d(x, \mu^2))^2$  in the valence region relevant at GSI kinematics, so that

$$\delta H(x_1, x_2; \mu^2) \simeq e_u^2 \delta u(x_1, \mu^2) \delta u(x_2, \mu^2) , \quad (12)$$

for (4). Hence the cross section (1) and the asymmetry (7) at GSI allow a direct access to  $|\delta u(x, \mu^2)|$ . The NLO transversities using (11) satisfy Soffer's inequality for the  $u$  quark, but violate it for the  $d$  quark by a small amount, see the last footnote and Figs. 1 (a), (b)<sup>§</sup>. However, this violation of Soffer's inequality will be harmless to our numerical estimates of the cross sections and asymmetries because of the dominance of the  $u$ -quark distribution noted above. We also mention that, strictly speaking, Soffer's inequality for the NLO distributions receives the additional scheme-dependent radiative corrections [5], and the corresponding corrections would modify the solid curve in Figs. 1 (a), (b) by a certain amount of  $\mathcal{O}(\alpha_s)$ .

In all the following numerical evaluation, we choose  $\phi = 0$  for the azimuthal angle of a lepton; extension to other  $\phi$  is straightforward by taking into account the  $\cos(2\phi)$  dependence displayed in the relevant formulae (1), (7), etc. For the nonperturbative parameter in (2) and (3), we use  $g_{NP} = 0.5 \text{ GeV}^2$  as used for the RHIC and J-PARC cases [13, 9, 10].

Probing the transversity distributions through the tDY in the collider mode is more promising than that in the fixed-target mode, because at higher energies the description based on QCD perturbation theory is supposed to be more accurate [12]. In Fig. 2(a), we show the  $Q_T$  spectrum of the dilepton in tDY with  $S = 210 \text{ GeV}^2$ ,  $Q = 4 \text{ GeV}$ , and  $y = 0$ , corresponding to a kinematics in the collider mode. We use the transversity distributions corresponding to the Soffer bound (the solid curve in Fig. 1), which were used in similar study of the  $Q_T$  spectrum at RHIC [13, 9, 10]. The solid line shows the spin-dependent part of the NLL+LO differential cross section (1), multiplied by  $2Q_T$ , and the dot-dashed line plots the contribution from the NLL resummed part  $\Delta_T \tilde{X}^{\text{NLL}}$  given in (2). The dotted line plots the contribution from the LL resummed part,

$$\Delta_T \tilde{X}^{\text{LL}}(Q_T^2, Q^2, y) = \left[ \int_{\mathcal{C}} db \frac{b}{2} J_0(bQ_T) e^{h^{(0)}(\lambda)/\alpha_s(Q^2) - g_{NP} b^2} \right] \delta H(x_1^0, x_2^0; Q^2) , \quad (13)$$

---

<sup>§</sup> The corresponding  $\bar{u}$ -,  $\bar{d}$ -, and  $\bar{s}$ -quark distributions satisfy Soffer's inequality.

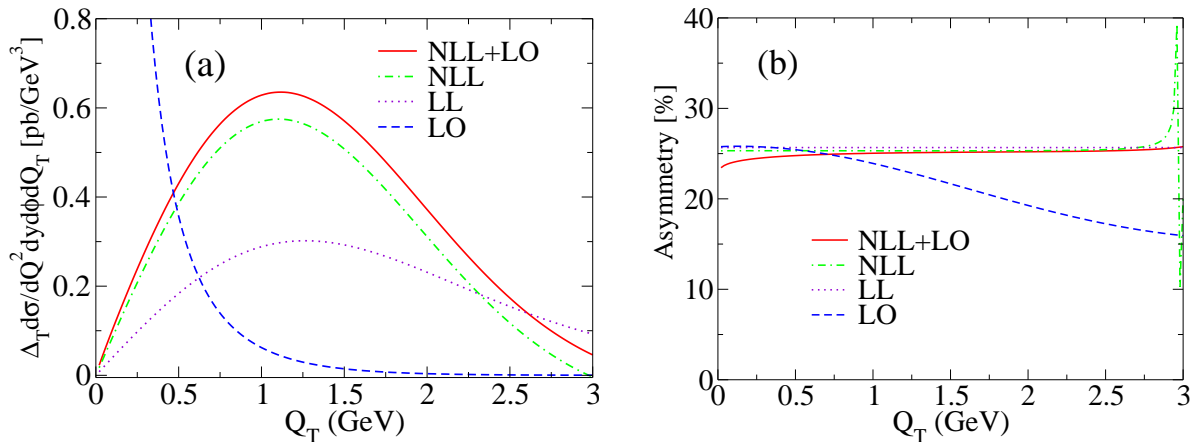


Figure 2: The tDY with GSI kinematics,  $S = 210 \text{ GeV}^2$ ,  $Q = 4 \text{ GeV}$ ,  $y = 0$  and  $\phi = 0$ , and with  $g_{NP} = 0.5 \text{ GeV}^2$ , using the NLO transversity distributions which correspond to the Soffer bound: (a) The spin-dependent part of the cross section,  $\Delta_T d\sigma/dQ^2 dQ_T dy d\phi$ . (b) The double transverse-spin asymmetries obtained using each curve in (a).

which is obtained from (2) by omitting the NLL terms with the nonperturbative inputs ( $g_{NP}$  and transversity distributions) kept intact; note that the  $b$  dependence of the parton distributions in (2) is associated with the NLL-level terms, as mentioned below (6) [9, 10, 14]. The dashed line shows the  $Q_T$  spectrum using the LO cross section  $\Delta_T d\sigma^{\text{LO}}/dQ^2 dQ_T^2 dy d\phi$  introduced above (7), which is divergent as  $Q_T \rightarrow 0$  due to the singular terms  $\propto \ln(Q^2/Q_T^2)/Q_T^2$ ,  $\propto 1/Q_T^2$ . By resumming the singular large logarithms to all orders in  $\alpha_s$ , the  $Q_T$  spectra are completely redistributed and well behaved, forming a peak at  $Q_T \sim 1 \text{ GeV}$ . In fact, around the peak region, the NLL+LO cross section is dominated by the contribution from the NLL resummed part  $\Delta_T \hat{X}^{\text{NLL}}$ . It is also remarkable that the NLL result is considerably enhanced compared with the LL result, though the integrations of these two results over  $Q_T$  coincide, using  $\lambda = 0$  at  $b = 0$  (see (6) and [9, 10]), up to the  $\mathcal{O}(\alpha_s(Q^2))$  corrections associated with the coefficient function  $\Delta_T C_{qq}^{(1)}$ . We note that the pattern similar to Fig. 2(a) is observed also in the corresponding  $Q_T$  spectra for the unpolarized differential cross sections.

The behavior of the NLL+LO cross section at  $Q_T \simeq 3 \text{ GeV}$  in Fig. 2(a) is still affected by the “broadening” due to the nonperturbative smearing  $e^{-g_{NP}b^2}$  in (2); as a result, the NLL+LO cross section is larger than the LO one at  $Q_T \simeq 3 \text{ GeV}$ , although the former was matched to the latter in the region where the logarithm  $\ln(Q^2/Q_T^2)$  is not large (see the discussion above (7)). Because the separation between the “peak region”  $Q_T \sim 1 \text{ GeV}$  and the “matching region”  $Q_T \sim Q$  is not so large for the present kinematics, the value  $Q_T \simeq 3 \text{ GeV}$  actually corresponds to the boundary between “smeared” and purely perturbative regimes. In fact, for higher  $\sqrt{S}$  and  $Q$  such that the peak and matching regions are largely separated, the NLL+LO cross section around  $Q_T \simeq Q$  is independent of the nonperturbative smearing and reduces to the LO one (see e.g. the results for RHIC in [13, 9, 10]). Another consequence due to the moderate-energy kinematics is that the perturbative contributions of



$\mathcal{O}(\alpha_s^2)$  and higher, involved in the NLL resummed component (2), are not negligible around  $Q_T \simeq Q$  at the quantitative level, as  $\alpha_s(Q^2)/\pi \sim 0.07$ . It is worth noting that, even in much higher energy processes such as  $Z$  boson [15] and Higgs boson productions [14], the higher-order perturbative contributions in the resummed component remain numerically sizable also at rather large  $Q_T$  well above the peak region. In the present case, however, the impact of those higher-order contributions can be even more significant, because the LO cross section at  $Q_T \sim Q$  is very small (see Fig. 2(a)); it is actually much smaller than its canonical size,  $[\alpha^2/3N_cSQ^2] \times [\alpha_s(Q^2)/\pi Q] \sim 10^{-2}$  pb/GeV<sup>3</sup> (see (1)), by the extra factor  $\sim 0.01$ ; here the extra small factor comes from the fact that, for the moderate energy  $\sqrt{S} = 14.5$  GeV, the  $2 \rightarrow 3$  partonic processes emitting a real gluon with the “high” transverse momentum  $k_T \sim Q$  are possible only from the initial-state partons with the large momentum fractions  $x_{1,2}$  as  $x_1x_2 \gtrsim 0.3$  ( $\gg Q^2/S$ ), for which the products of the parton distributions in (4) are strongly suppressed (see Fig. 1). These points suggest that the accurate quantitative description around  $Q_T \simeq Q$  at GSI would eventually require the matching procedure taking into account also the  $\mathcal{O}(\alpha_s^2)$  or higher contributions in perturbation theory, which is beyond our NLL+LO framework. One may expect that the mechanisms observed for the large  $Q_T$  region in the “NLL+NLO” cross section of  $Z$  boson production [15] and in the “NNLL+NLO” cross section of Higgs boson production [14] could also provide a better treatment for the matching region  $Q_T \sim Q$  in the present case. Nevertheless, in this paper, we insist on the NLL+LO framework because the tDY  $Q_T$ -differential cross section is not known at NLO, and we restrict our quantitative discussion below the matching region.

Figure 2(b) shows the asymmetries as functions of  $Q_T$ , obtained by taking the ratio of each curve in Fig.2(a) to the corresponding  $Q_T$  spectra for the unpolarized cross sections; i.e., the solid, dot-dashed, and dashed curves plot the NLL+LO ( $\mathcal{A}_{TT}(Q_T)$  of (7)), NLL ( $\mathcal{A}_{TT}^{\text{NLL}}(Q_T)$  of (8)), and LO ( $\mathcal{A}_{TT}^{\text{LO}}(Q_T)$  below (7)) asymmetries, respectively, and the dotted curve shows the LL asymmetry, obtained by using (13) and the similar formula for  $\tilde{X}^{\text{LL}}$ , as

$$\mathcal{A}_{TT}^{\text{LL}} = \frac{1}{2} \cos(2\phi) \frac{\Delta_T \tilde{X}^{\text{LL}}(Q_T^2, Q^2, y)}{\tilde{X}^{\text{LL}}(Q_T^2, Q^2, y)} = \frac{1}{2} \cos(2\phi) \frac{\delta H(x_1^0, x_2^0; Q^2)}{H(x_1^0, x_2^0; Q^2)}, \quad (14)$$

which is constant in  $Q_T$ . All asymmetries in Fig. 2(b), except the LO result, show similar flat behavior with almost the same value  $\simeq 25\%$ . The results observed in Fig. 2(a) imply that these flat behaviors are governed by the soft gluon resummation contributions. In particular, we have, for  $Q_T$  around the peak region in Fig. 2(a),

$$\mathcal{A}_{TT}(Q_T) \simeq \mathcal{A}_{TT}^{\text{NLL}}(Q_T) \simeq \mathcal{A}_{TT}^{\text{NLL}}(0), \quad (15)$$

and the flat behavior, represented by the second (approximate) equality, reflects the fact that the soft gluon effects resummed into the Sudakov factor  $e^{S(b,Q)}$  are universal to the NLL accuracy between  $\Delta_T \tilde{X}^{\text{NLL}}$  and  $\tilde{X}^{\text{NLL}}$  in (8). In fact, similar flat behavior is observed in  $pp$  collisions at RHIC and J-PARC kinematics [9, 10]; note, remarkably, the present result for  $p\bar{p}$  collisions turns out to be even flatter. As  $Q_T \rightarrow 0$ , away from the peak region of the cross section,  $\mathcal{A}_{TT}(Q_T)$  decreases slightly due to the terms  $\propto \ln(Q^2/Q_T^2)/Q^2$  contained in  $\Delta_T \tilde{Y}$  and  $\tilde{Y}$  in (7). The difference between  $\mathcal{A}_{TT}(Q_T)$  and the LO asymmetry at  $Q_T \simeq 3$  GeV reflects the above-mentioned discrepancy between the corresponding cross sections.

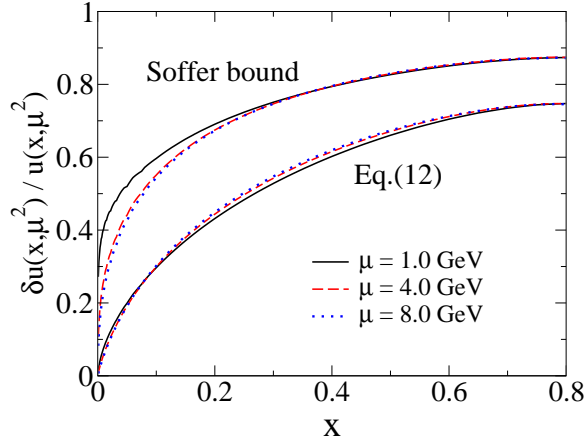


Figure 3: The ratio of the transversity to unpolarized quark distribution for  $u$ -quark at different scales  $\mu$ . The upper and lower curves are obtained using the NLO transversity distributions corresponding to the Soffer bound and the relation (11), respectively.

We here recall that, in the  $pp$ -collision cases at RHIC and J-PARC using the same input transversity distributions as in Fig. 2(b), the significant enhancement of  $\mathcal{A}_{TT}^{\text{NLL}}(Q_T)$  ( $\simeq \mathcal{A}_{TT}(Q_T)$ ) compared with  $\mathcal{A}_{TT}^{\text{LL}}$  has been found [9, 10]. Such enhancement is not seen in the present  $p\bar{p}$ -collision case. This fact indicates that the large NLL-level corrections shown in Fig. 2(a) are canceled in the asymmetry  $\mathcal{A}_{TT}^{\text{NLL}}(Q_T)$  with the corresponding corrections to the unpolarized cross section, although this is not the case in the  $pp$  collisions.

To clarify the reason behind this remarkable difference between the  $p\bar{p}$ - and  $pp$ -collision cases, the saddle-point formula (10) is useful. Similarly to the  $pp$ -collision case [9, 10], the property (15) allows us to use (10) as a sufficiently accurate estimation of  $\mathcal{A}_{TT}(Q_T)$ ,  $\mathcal{A}_{TT}^{\text{NLL}}(Q_T)$  (see Fig. 4 and Table 1 below). We obtain  $b_0/b_{SP} = 1.0$  GeV for the scale of the transversity and unpolarized distributions in the numerator and denominator of (10) at the kinematics of Fig. 2, using the condition that was noted below (9)<sup>¶</sup>.  $\mathcal{A}_{TT}^{\text{LL}}$  of (14) is different from (10), only in the scale  $Q$  ( $= 4$  GeV for Fig. 2) of the parton distributions. Therefore, the possible enhancement of  $\mathcal{A}_{TT}(Q_T)$ ,  $\mathcal{A}_{TT}^{\text{NLL}}(Q_T)$  in comparison with  $\mathcal{A}_{TT}^{\text{LL}}$  can be understood as a result of QCD evolution of the parton distributions from  $b_0/b_{SP}$  to  $Q$ , with  $Q^2 \gg b_0^2/b_{SP}^2$ : in fact, the corresponding enhancement in  $pp$  collisions at RHIC and J-PARC arises because of very different behavior of the sea-quark components under the evolution between transversity and unpolarized distributions [9, 10]; note that the transversity distributions obey a non-singlet-type evolution even for the sea-quark components because there is no gluon transversity distribution. On the other hand, in  $p\bar{p}$  collisions at GSI, associated with the region  $0.2 \lesssim x_{1,2}^0 \lesssim 0.7$ , the relevant formulae (10), (14) for the asymmetries are

<sup>¶</sup> The value of  $b_0/b_{SP}$  in principle depends on the input values for  $Q$  and  $g_{NP}$ , but in practice  $b_0/b_{SP} \simeq 1$  GeV, irrespective of  $Q$  and  $g_{NP}$  (see [9, 10] for the detail). This in turn implies that (10), and thus  $\mathcal{A}_{TT}(Q_T)$  as well as  $\mathcal{A}_{TT}^{\text{NLL}}(Q_T)$ , are almost independent of the value of  $g_{NP}$ . We have explicitly checked this point also in the direct numerical evaluation of (7) with (2), (3) in the range  $g_{NP} = 0.3\text{--}0.8$  GeV<sup>2</sup>.

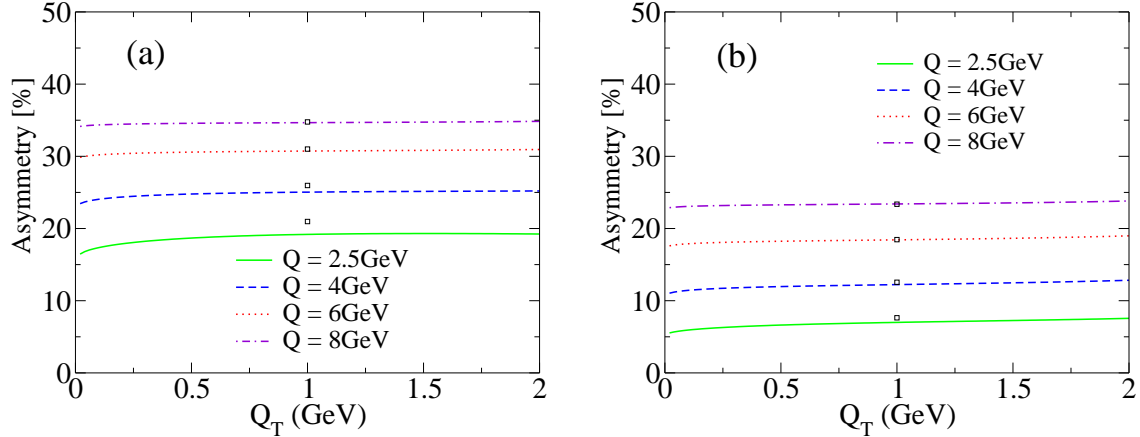


Figure 4: The NLL+LO asymmetry  $\mathcal{A}_{TT}(Q_T)$  of (7) with GSI kinematics,  $S = 210 \text{ GeV}^2$  and  $y = \phi = 0$ , and with  $g_{NP} = 0.5 \text{ GeV}^2$ , using the NLO transversity distributions corresponding to (a) the Soffer bound and (b) the relation (11), respectively. The corresponding values of the saddle-point formula (10) are also shown by the symbols at  $Q_T = 1 \text{ GeV}$ .

dominated by the contributions from the valence components, such that

$$\mathcal{A}_{TT}(Q_T) \simeq \mathcal{A}_{TT}^{\text{NLL}}(Q_T) \simeq \frac{1}{2} \cos(2\phi) \frac{\delta u(x_1^0, b_0^2/b_{SP}^2) \delta u(x_2^0, b_0^2/b_{SP}^2)}{u(x_1^0, b_0^2/b_{SP}^2) u(x_2^0, b_0^2/b_{SP}^2)}, \quad (16)$$

and  $\mathcal{A}_{TT}^{\text{LL}} \simeq [\cos(2\phi)/2][\delta u(x_1^0, Q^2) \delta u(x_2^0, Q^2)/u(x_1^0, Q^2) u(x_2^0, Q^2)]$ , using (12) and the similar relation for the unpolarized distributions (see (4)). As demonstrated in Fig. 3, the scale dependence of the  $u$ -quark distributions cancels between the numerator and denominator of (16) in the relevant “valence region”. This fact explains why  $\mathcal{A}_{TT}(Q_T) \simeq \mathcal{A}_{TT}^{\text{NLL}}(Q_T) \simeq \mathcal{A}_{TT}^{\text{LL}}$  in Fig. 2(b). We note that actually the same mechanism arises for all kinematics at GSI, and also for the input transversity distributions using (11) (see Fig. 3). This implies that the property,  $\mathcal{A}_{TT}(Q_T) \simeq \mathcal{A}_{TT}^{\text{NLL}}(Q_T) \simeq \mathcal{A}_{TT}^{\text{LL}}$ , is characteristic of all  $p\bar{p}$  collisions at GSI. Moreover, a similar logic applied to (2) allows us to derive the second approximate equality of (15): using (12) and the property  $\delta u(x_{1,2}^0, b_0^2/b^2) \simeq u(x_{1,2}^0, b_0^2/b^2) \delta u(x_{1,2}^0, b_0^2/b_{SP}^2)/u(x_{1,2}^0, b_0^2/b_{SP}^2)$  implied by Fig. 3, (2) gives  $\Delta_T \tilde{X}^{\text{NLL}}(Q_T^2, Q^2, y) \simeq [\delta u(x_1^0, b_0^2/b_{SP}^2) \delta u(x_2^0, b_0^2/b_{SP}^2)/u(x_1^0, b_0^2/b_{SP}^2) u(x_2^0, b_0^2/b_{SP}^2)] \tilde{X}^{\text{NLL}}(Q_T^2, Q^2, y)$ , up to the  $\mathcal{O}(\alpha_s)$  corrections associated with the coefficient functions  $(\Delta_T) C_{ij}^{(1)}(z)$  in (2) and (3). This immediately gives the second relation in (15), combined with (8) and (10). This derivation using the properties in the valence region also explains why  $\mathcal{A}_{TT}(Q_T)$ ,  $\mathcal{A}_{TT}^{\text{NLL}}(Q_T)$  in  $p\bar{p}$  collisions at GSI are flatter than in  $pp$  collisions as noted below (15) (see also Figs. 4-7 below).

Using the same nonperturbative and kinematical inputs as in Fig. 2, Fig. 4(a) shows the dependence of the NLL+LO asymmetry  $\mathcal{A}_{TT}(Q_T)$  of (7) on the dilepton mass  $Q$ ; the dashed curve in Fig. 4(a) is the same as the solid curve in Fig. 2(b), and the results in Fig. 4(a) show the “maximally possible” asymmetry, i.e., should be considered as optimistic estimate (see the solid curve in Fig. 1). We expect that a more realistic estimate is provided by the

	Soffer bound				Eq. (11)			
$Q$	2.5GeV	4GeV	6GeV	8GeV	2.5GeV	4GeV	6GeV	8GeV
SP	21.0%	26.0%	31.0%	34.8%	7.6%	12.6%	18.5%	23.4%
NB	19.6%	25.3%	30.8%	34.7%	7.2%	12.4%	18.5%	23.4%

Table 1: The values of  $\mathcal{A}_{TT}^{\text{NLL}}(Q_T = 0)$  of (8) for the cases of Figs. 4 (a) and (b), as ‘‘Soffer bound’’ and ‘‘Eq. (11)’’, respectively. SP is obtained using the saddle-point formula (10) and NB is obtained using the numerical  $b$ -integration of (2) and (3).

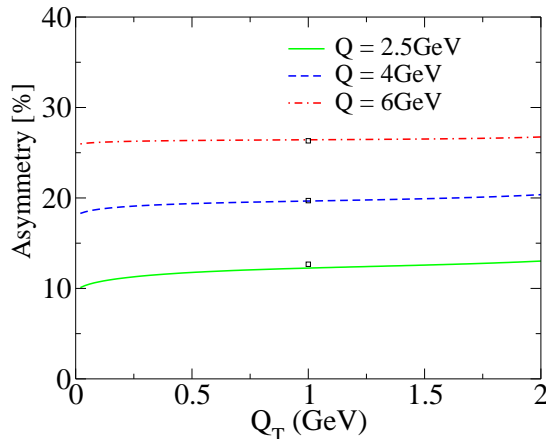


Figure 5: Same as Fig. 4(b), but for  $S = 80 \text{ GeV}^2$ .

results in Fig. 4(b), which is same as Fig. 4(a) but for the case with the input transversity distributions using (11) corresponding to the dashed curve in Fig. 1. As  $Q$  increases,  $\mathcal{A}_{TT}(Q_T)$  increase, preserving the characteristic flat behavior as functions of  $Q_T$ . The results in Fig. 4(b) using (11) are smaller compared with the corresponding Soffer bound results in Fig. 4(a), but still yield rather large asymmetries.

The saddle-point formula (10) has a particularly simple structure, including only the parton distribution functions at the fixed values  $x = x_{1,2}^0$  and at a single scale  $b_0/b_{SP} \simeq 1 \text{ GeV}$ , and, combined with (15), allows us to obtain  $\mathcal{A}_{TT}(Q_T)$  at  $Q_T \simeq 1 \text{ GeV}$ . In Table 1, the row labeled ‘‘SP’’ lists the results<sup>||</sup> obtained using the saddle-point formula (10), with the kinematics and nonperturbative inputs of Figs. 4 (a) and (b); for convenience, the corresponding values are plotted by the symbol ‘‘□’’ at  $Q_T = 1 \text{ GeV}$  in Figs. 4 (a) and (b). ‘‘NB’’ in Table 1 lists  $\mathcal{A}_{TT}^{\text{NLL}}(Q_T = 0)$  obtained from (8) using the numerical  $b$ -integration of (2) and (3). We observe that the simple formula (10) has indeed the remarkable accuracy, reproducing the results of NB as well as the NLL+LO  $\mathcal{A}_{TT}(Q_T)$  to 10% accuracy, i.e., to the canonical size of  $\mathcal{O}(\alpha_s)$  corrections associated with the NLL accuracy (see the discussion below (9)). We also emphasize that the saddle-point formula (10) indicates that the  $Q$

<sup>||</sup> These results correspond to ‘‘SP-II’’ discussed in [9, 10].

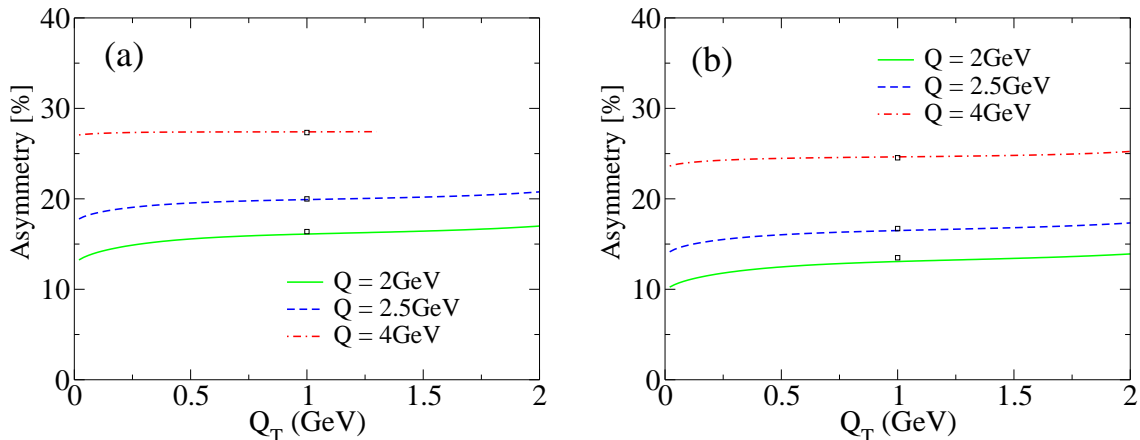


Figure 6: Same as Fig. 4(b), but for (a)  $S = 30 \text{ GeV}^2$  and (b)  $S = 45 \text{ GeV}^2$ .

dependence of  $\mathcal{A}_{TT}(Q_T)$  is controlled by the detailed  $x_{1,2}^0$  dependence of the transversity and density distributions at the scale  $b_0/b_{SP}$ . Namely the  $Q$  dependence in Fig. 4 can be understood by the behavior of the solid lines in Fig. 3 using (16).

In Fig. 5, we show the NLL+LO asymmetry  $\mathcal{A}_{TT}(Q_T)$  of (7) at another kinematics in the collider mode,  $S = 80 \text{ GeV}^2$  and  $y = 0$ , with the transversity distributions using (11). The results are displayed similarly as Fig. 4. The observed pattern is similar as Fig. 4(b), but the asymmetries are considerably larger.

Figure 6 shows the NLL+LO asymmetries  $\mathcal{A}_{TT}(Q_T)$  in the fixed-target mode, which is associated with more challenging kinematic regime for the application of QCD factorization framework: (a) and (b) plot the results for  $S = 30$  and  $45 \text{ GeV}^2$ , respectively, with  $y = 0$  using (11). The dot-dashed curve in (a) ends at the kinematical upper bound for the partonic subprocess,  $Q_{T,\text{max}} = Q\sqrt{[1 - (x_1^0)^2][1 - (x_2^0)^2]/(x_1^0 + x_2^0)} = 1.3 \text{ GeV}$ ; because of this kinematical bound, we do not show the cases with  $Q$  higher than 4 GeV. Compared to (a), the case (b) probes smaller  $x_{1,2}^0$  region, resulting in the smaller asymmetries. Both results give larger asymmetries than the corresponding collider results with the same  $Q$ . The characteristic behaviors as functions of  $Q_T$  and  $Q$  emphasized above are again observed, and actually the specific contributions associated with the results in Fig. 6 obey similar pattern as in Figs. 2 (a) and (b), with e.g.,  $\mathcal{A}_{TT}(Q_T) \simeq \mathcal{A}_{TT}^{\text{NLL}}(Q_T) \simeq \mathcal{A}_{TT}^{\text{LL}}$ .

We mention the rapidity dependence of the NLL+LO asymmetry (7). Figures 7 (a) and (b) are same as Figs. 4(b) and 6(b) in the collider and fixed-target modes, respectively, but for  $y = 0.5$  and  $0.3$ , and all results agree nicely with the saddle-point results using (10). The characteristic behaviors common to the preceding results are again observed, but the values of asymmetry are slightly smaller than the corresponding values for  $y = 0$ .

Figure 8 summarizes our results for the double transverse-spin asymmetry  $\mathcal{A}_{TT}(Q_T)$  of (7) at GSI as functions of the dilepton mass  $Q$  with  $y = 0$  and various values of  $S$  corresponding to the fixed-target as well as collider mode. The symbols “ $\Delta$ ” and “ $\nabla$ ” plot  $\mathcal{A}_{TT}(Q_T = Q_{T,\text{peak}})$  using the NLO transversity distributions corresponding to the

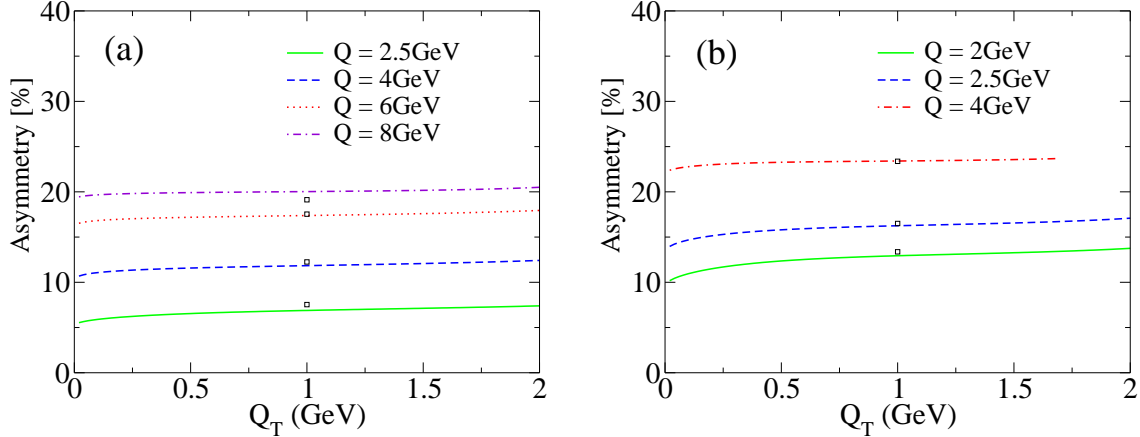


Figure 7: (a) Same as Fig. 4(b), but for  $y = 0.5$ . (b) Same as Fig. 6(b), but for  $y = 0.3$ .

Soffer bound and (11), respectively, where  $Q_{T,\text{peak}}$  denotes the value of  $Q_T$  at which the peak of the corresponding NLL+LO tDY cross section is located (see Fig. 2(a)); e.g., the several symbols “ $\nabla$ ” in Figs. 8 (a), (b), (c), and (d) denote the values of the curves at  $Q_T = Q_{T,\text{peak}} (\simeq 1 \text{ GeV})$  in Figs. 6(a), 6(b), 5 and 4(b), respectively. The dashed and dot-dashed curves draw the results of the saddle-point formula (10) using the same parton distributions as those for “ $\Delta$ ” and “ $\nabla$ ”, respectively. The results remind the readers of the relation (15). Combined with the result in Fig. 3, this relation convinces us that the property,  $\mathcal{A}_{TT}(Q_T) \simeq \mathcal{A}_{TT}^{\text{NLL}}(Q_T) \simeq \mathcal{A}_{TT}^{\text{LL}}$ , which was discussed below (16), indeed holds at all relevant kinematics at GSI.

The conventional double transverse-spin asymmetry  $A_{TT}$  is defined as the ratio of the  $Q_T$ -integrated polarized and unpolarized DY cross sections, and  $A_{TT}$  at GSI kinematics has been studied in previous works [7, 11, 12]. It is worth noting the relation of  $A_{TT}$  with our  $Q_T$ -dependent asymmetry  $\mathcal{A}_{TT}(Q_T)$ . As explicitly demonstrated in [10], the integral of (1) over  $Q_T$  reproduces *exactly* the corresponding NLO cross sections for the  $Q_T$ -unobserved case; indeed  $\lambda = 0$  at  $b = 0$  in (6) ensures [13, 9, 14] that the contributions of  $\mathcal{O}(\alpha_s^2)$  or higher from the resummed components (2), (3) vanish in the  $Q_T$  integral. As a result,

$$A_{TT} \equiv \frac{\int dQ_T^2 (\Delta_T d\sigma/dQ^2 dQ_T^2 dy d\phi)}{\int dQ_T^2 (d\sigma/dQ^2 dQ_T^2 dy d\phi)} = \frac{1}{2} \cos(2\phi) \frac{\delta H(x_1^0, x_2^0; Q^2) + \dots}{H(x_1^0, x_2^0; Q^2) + \dots}, \quad (17)$$

where the ellipses stand for the NLO correction terms, coincides completely with the NLO asymmetry calculated in [11]. It has been found [11] that the effects of the ellipses in (17) on  $A_{TT}$  are generally small at GSI; i.e., the corresponding  $K$  factors of the polarized and unpolarized cross sections are similar to each other and cancel out in the ratio. Indeed the LO contribution shown explicitly in (17) coincides with (14), i.e.,  $A_{TT}^{\text{LO}} = \mathcal{A}_{TT}^{\text{LL}}$ , while the NLO calculation yields e.g.,  $A_{TT} = 25.0\%$  for the case of Fig. 2(b).

In view of the fact  $A_{TT} \simeq A_{TT}^{\text{LO}}$  at GSI, it is also interesting to calculate the conventional LO asymmetry  $A_{TT}^{\text{LO}}$  using the LO transversity distributions, obtained by Anselmino et al. [4]

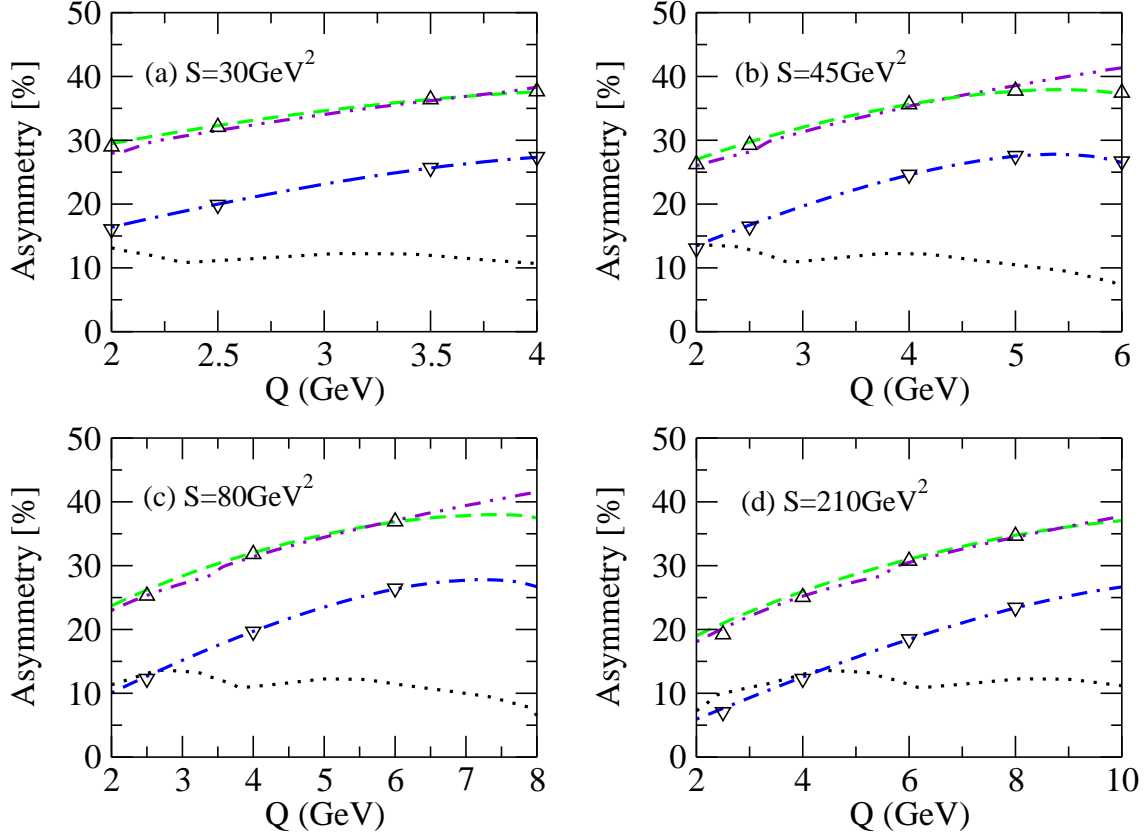


Figure 8: The double transverse-spin asymmetries as functions of  $Q$  at  $y = 0$ . The dashed and dot-dashed curves plot the results of the saddle-point formula (10), using the NLO transversities corresponding to the Soffer bound and (11), respectively, which yield the values of  $\mathcal{A}_{TT}(Q_T)$  of (7) for  $Q_T = Q_{T,\text{peak}} (\simeq 1 \text{ GeV})$  as indicated by the triangle up and down symbols. The two-dot-dashed curve shows the conventional  $Q_T$ -independent LO asymmetry  $A_{TT}^{\text{LO}}$  using the LO transversities corresponding to the Soffer bound. The dotted curve shows the “upper bound” of  $A_{TT}^{\text{LO}}$  implied by the result of the global fit in [4].

through the global fit to the data. (For the unpolarized distributions in the denominator of  $A_{TT}^{\text{LO}}$ , we use LO GRV98 distributions [19].) The upper limit of the one-sigma error bounds of their fitted transversities (shaded area in Fig. 1) yields the “upper bound” of the corresponding  $A_{TT}^{\text{LO}}$  as shown by the dotted curves in Fig. 8. Also plotted by the two-dot-dashed curves are  $A_{TT}^{\text{LO}}$  using the LO transversity distributions corresponding to the Soffer bound, which are given by the dot-dashed curves in Fig. 1. We here note that the above mentioned relations,  $\mathcal{A}_{TT}(Q_T) \simeq \mathcal{A}_{TT}^{\text{NLL}}(Q_T) \simeq \mathcal{A}_{TT}^{\text{LL}}$  and  $A_{TT}^{\text{LO}} = \mathcal{A}_{TT}^{\text{LL}}$ , imply  $\mathcal{A}_{TT}(Q_T) \simeq A_{TT}^{\text{LO}}$ . Therefore, the dotted curves in Fig. 8 represent not only estimate of  $A_{TT}$ , but also that of  $\mathcal{A}_{TT}(Q_T \sim Q_{T,\text{peak}})$ , using the empirical information of the transversities available at present, up to anticipated modification of the empirical transversities at the NLO level. The effect of the corresponding NLO-level modification of the input transversities on the

asymmetries might not be so large, as suggested by the fact that the dashed curve in each panel of Fig. 8 is close to the corresponding two-dot-dashed curve. In the small  $Q$  region, our full result of  $\mathcal{A}_{TT}(Q_T)$  using (11) can be consistent with estimate using the empirical LO transversities, but these results have rather different behavior for increasing  $Q$ , which reflects the different  $x$ -dependence of the corresponding transversities shown in Fig. 1. This demonstrates that the experimental data to be observed at GSI, in particular the behavior of the  $Q_T$ -dependent as well as  $Q_T$ -independent asymmetries as functions of  $Q$ , will allow us to determine the detailed shape of the transversity distributions in the valence region.

To summarize, the double transverse-spin asymmetry at a measured  $Q_T$  to be observed at GSI is very useful to determine the transversity, and is complementary to the conventional asymmetry associated with the  $Q_T$ -integrated cross sections: both asymmetries are large at GSI, and actually the values of these two asymmetries are almost the same for all GSI kinematics. This (approximate) “equality” of the two asymmetries is unexpected from the outset and characteristic of  $p\bar{p}$  collisions in GSI experiments, and we have revealed nontrivial roles played by the soft-gluon-resummation contributions. Indeed, only after performing the soft gluon resummation, we obtain the “physical” behavior for the  $Q_T$  spectra of the DY lepton pair and the associated asymmetry  $\mathcal{A}_{TT}(Q_T)$  in the small  $Q_T$  region, with a well-developed peak for the former and the flat behavior for the latter, and thus we are able to make the reliable estimate. Furthermore, the resummation modifies the parton distributions involved in  $\mathcal{A}_{TT}(Q_T)$  into those with the “effective” scale around  $Q_T \sim 1$  GeV, instead of  $Q$  in the conventional asymmetry. Another reason for the above “equality” is the similarity of the QCD evolution between the transversity and unpolarized quark distributions in the valence region relevant to the GSI kinematics. These mechanisms have been explicitly embodied by the novel saddle-point formula, which relates the asymmetry  $\mathcal{A}_{TT}(Q_T)$  with the transversity distributions at the scale around 1 GeV, in a way as simple as in the conventional LO asymmetry. Thus GSI measurements of the asymmetries at a small  $Q_T$  for a variety of dilepton mass  $Q$  directly probe the shape of the transversity distributions.

## Acknowledgments

We thank Werner Vogelsang, Hiroshi Yokoya and Stefano Catani for valuable discussions. We also thank Mauro Anselmino and Alexei Prokudin for helpful discussions on their results in [4]. This work was supported by the Grant-in-Aid for Scientific Research No. B-19340063.

## References

- [1] J. P. Ralston and D. E. Soper, Nucl. Phys. **B152** (1979) 109; R. L. Jaffe and X. D. Ji, *ibid.* **B375** (1992) 527; J. L. Cortes, B. Pire and J. P. Ralston, Z. Phys. **C55** (1992) 409.
- [2] See e.g., V. Barone, A. Drago and P. G. Ratcliffe, Phys. Rept. **359** (2002) 1; J. Kodaira and K. Tanaka, Prog. Theor. Phys. **101** (1999) 191.



- [3] M. Göckeler et al. [QCDSF/UKQCD Collaboration], Phys. Lett. **B627** (2005) 113; M. Diehl et al. [QCDSF/UKQCD Collaboration], hep-ph/0511032.
- [4] M. Anselmino, M. Boglione, U. D'Alesio, A. Kotzinian, F. Murgia, A. Prokudin and C. Turk, Phys. Rev. **D75** (2007) 054032.
- [5] J. Soffer, Phys. Rev. Lett. **74** (1995) 1292; G. R. Goldstein, R. L. Jaffe and X. D. Ji, Phys. Rev. **D52** (1995) 5006.
- [6] V. Barone et al. [PAX Collaboration], hep-ex/0505054; M. Maggiora et al. [ASSIA Collaboration], hep-ex/0504011.
- [7] M. Anselmino, V. Barone, A. Drago and N. N. Nikolaev, Phys. Lett. **B594** (2004) 97; A. V. Efremov, K. Goeke and P. Schweitzer, Eur. Phys. J. **C35** (2004) 207.
- [8] O. Martin, A. Schäfer, M. Stratmann and W. Vogelsang, Phys. Rev. **D57** (1998) 3084; *ibid.* **D60** (1999) 117502.
- [9] H. Kawamura, J. Kodaira and K. Tanaka, Nucl. Phys. **B777** (2007) 203.
- [10] H. Kawamura, J. Kodaira and K. Tanaka, Prog. Theor. Phys. **118** (2007) 581 [arXiv:0709.1752 [hep-ph]].
- [11] V. Barone, A. Cafarella, C. Coriano, M. Guzzi and P. G. Ratcliffe, Phys. Lett. **B639** (2006) 483.
- [12] H. Shimizu, G. Sterman, W. Vogelsang and H. Yokoya, Phys. Rev. **D71** (2005) 114007.
- [13] H. Kawamura, J. Kodaira, H. Shimizu and K. Tanaka, Prog. Theor. Phys. **115** (2006) 667.
- [14] S. Catani, D. de Florian and M. Grazzini, Nucl. Phys. **B596** (2001) 299; G. Bozzi, S. Catani, D. de Florian and M. Grazzini, Phys. Lett. **B564** (2003) 65; Nucl. Phys. **B737** (2006) 73; *ibid.* **B791** (2007) 1.
- [15] E. Laenen, G. Sterman and W. Vogelsang, Phys. Rev. **D63** (2001) 114018; A. Kulesza, G. Sterman and W. Vogelsang, *ibid.* **D66** (2002) 014011.
- [16] J. C. Collins, D. Soper and G. Sterman, Nucl. Phys. **B250** (1985) 199.
- [17] J. Kodaira and L. Trentadue, Phys. Lett. **B112** (1982) 66; Report **SLAC-Pub-2934** (1982); Phys. Lett. **B123** (1983) 335; C. T. H. Davies, W. J. Stirling, Nucl. Phys. **B244** (1984) 337.
- [18] G. Parisi and R. Petronzio, Nucl. Phys. **B154** (1979) 427; J. C. Collins and D. E. Soper, *ibid.* **B197** (1982) 446.
- [19] M. Glück, E. Reya and A. Vogt, Eur. Phys. J. **C5** (1998) 461.

- [20] M. Glück, E. Reya, M. Stratmann, and W. Vogelsang, Phys. Rev. **D63** (2001) 094005.
- [21] A. Hayashigaki, Y. Kanazawa and Y. Koike, Phys. Rev. **D56** (1997) 7350; S. Kumano and M. Miyama, *ibid.* **D56** (1997) 2504; W. Vogelsang, *ibid.* **D57** (1998) 1886.
- [22] For recent model calculations, see e.g., M. Wakamatsu, Phys. Lett. **B653** (2007) 398; B. Pasquini, M. Pincetti and S. Boffi, Phys. Rev. **D76** (2007) 034020; I. C. Cloët, W. Bentz and A. W. Thomas, Phys. Lett. **B659** (2008) 214.